3D high- and super-resolution imaging using single-objective SPIM

Remi Galland[1–3], Gianluca Grenci[3], Ajay Aravind[3], Virgile Viasnoff[3–6], Vincent Studer[1,2,6] & Jean-Baptiste Sibarita[1,2,6]

Single-objective selective-plane illumination microscopy (soSPIM) is achieved with micromirrored cavities combined with a laser beam–steering unit installed on a standard inverted microscope. The illumination and detection are done through the same objective. soSPIM can be used with standard sample preparations and features high background rejection and efficient photon collection, allowing for 3D single-molecule-based super-resolution imaging of whole cells or cell aggregates. Using larger mirrors enabled us to broaden the capabilities of our system to image *Drosophila* embryos.

Over the past decade, selective-plane illumination microscopy (SPIM) has demonstrated its superior capacity to image thick, live samples in 3D for a prolonged duration compared to wide-field, confocal or multiphoton-excitation microscopy. This technique has been widely used in developmental biology for 4D reconstructions of live embryos and thick tissues. SPIM is usually achieved through the use of two objectives arranged perpendicular to each other—one for generating a planar illumination, and the other for collecting fluorescence. SPIM's high sectioning capability, high contrast, reduced photo-bleaching and reduced phototoxicity relative to other approaches are appealing properties for 3D single-molecule-based nanoscopy. Single-molecule-based super-resolution microscopy is usually constrained to 2D observation at the surface of the glass coverslip using total internal reflection fluorescence illumination. By combining oblique illumination[1] and point-spread-function engineering methods[2,3] or biplane imaging[4], one can obtain 3D images of material within the first micrometer above the coverslip, with an axial resolution less than 50 nm. Interferometric techniques such as interferometric photoactivated localization microscopy (PALM) use two objectives in a 4Pi illumination configuration and improve the axial resolution below 10 nm (ref. 5), but the constraints on imaging depth are similar to those associated with the previously mentioned methods. In special cases, when proteins are confined in cellular regions, single-molecule-based nanoscopy of structures deeper inside biological samples can be achieved[4]. Combining SPIM illumination with single-molecule detection is a good alternative[6–12], but it always requires a complicated and non-versatile two-objective-based experimental setup.

Here we show how a single objective can be used to produce SPIM 3D optical sectioning with capabilities ranging from single-molecule detection at the cellular level to whole-embryo imaging.

soSPIM relies on the reflection of an excitation beam onto a 45° mirror to create a light sheet perpendicular to the optical axis, with fluorescent light collected through the same objective used to generate the illumination (**Fig. 1a,b**). We created a multi-wavelength light sheet either by using a cylindrical lens placed in the excitation path or by means of linear scanning along the *y*-axis of the mirror. By steering the beam along the *x*-axis of the mirror, we controlled the axial position of the illumination plane along the *z*-direction. We matched the objective's focal plane with the illumination plane (**Supplementary Fig. 1**) and positioned the thinnest part of the light sheet across the sample by defocusing the incoming laser using an electrically driven tunable divergent lens (**Supplementary Fig. 2a**). We were able to adjust the thickness and length of the light sheet with an exchangeable telescope that tuned the size of the Gaussian beam in the back focal plane of the objective. We achieved sizes ranging from $265 \times 500 \times 5.2\ \mu m^3$ (length × width × thickness) to $13 \times 30 \times 1.2\ \mu m^3$ with objectives ranging from 10×/0.3 numerical aperture (NA) to 100×/1.3 NA working at distances between 10 and 600 µm from the 45° mirror (**Supplementary Fig. 2b–d**). We used the same tunable lens to synchronously compensate for the translation of the beam waist along the *x*-axis upon axial displacement of the objective (**Supplementary Fig. 3**).

The light-sheet thickness compared favorably with values obtained for single-cell SPIM[6–12] (**Supplementary Table 1**) using high-NA objectives. The 60-kHz scanning speed of the galvanometric mirrors and the 500-Hz response time of the tunable lens were fast enough that the acquisition frame rate was limited solely by the sample brightness and the camera's maximum acquisition speed.

In addition to the beam-steering unit, the fabrication of the mirrors is important to our technique. We molded disposable micromirror chips by imprinting a master mold in a UV-curable polymer (NOA 73 or MYpoly134). We adjusted the dimensions of the mirrors according to the size of the samples (**Supplementary Fig. 4**) and used two different protocols to fabricate cavities for cell (20–200 µm) and embryo (700 nm to 3 mm) imaging (Online

[1]Interdisciplinary Institute for Neuroscience, University of Bordeaux, Bordeaux, France. [2]Centre National de la Recherche Scientifique, Bordeaux, France. [3]Mechanobiology Institute, National University of Singapore, Singapore. [4]Bio Mechanics of Cellular Contacts, Centre National de la Recherche Scientifique, Singapore. [5]Department of Biological Science, National University of Singapore, Singapore. [6]These authors contributed equally to this work. Correspondence should be addressed to V.V. (dbsvvnr@nus.edu.sg).

RECEIVED 15 AUGUST 2014; ACCEPTED 12 APRIL 2015; PUBLISHED ONLINE 11 MAY 2015; DOI:10.1038/NMETH.3402

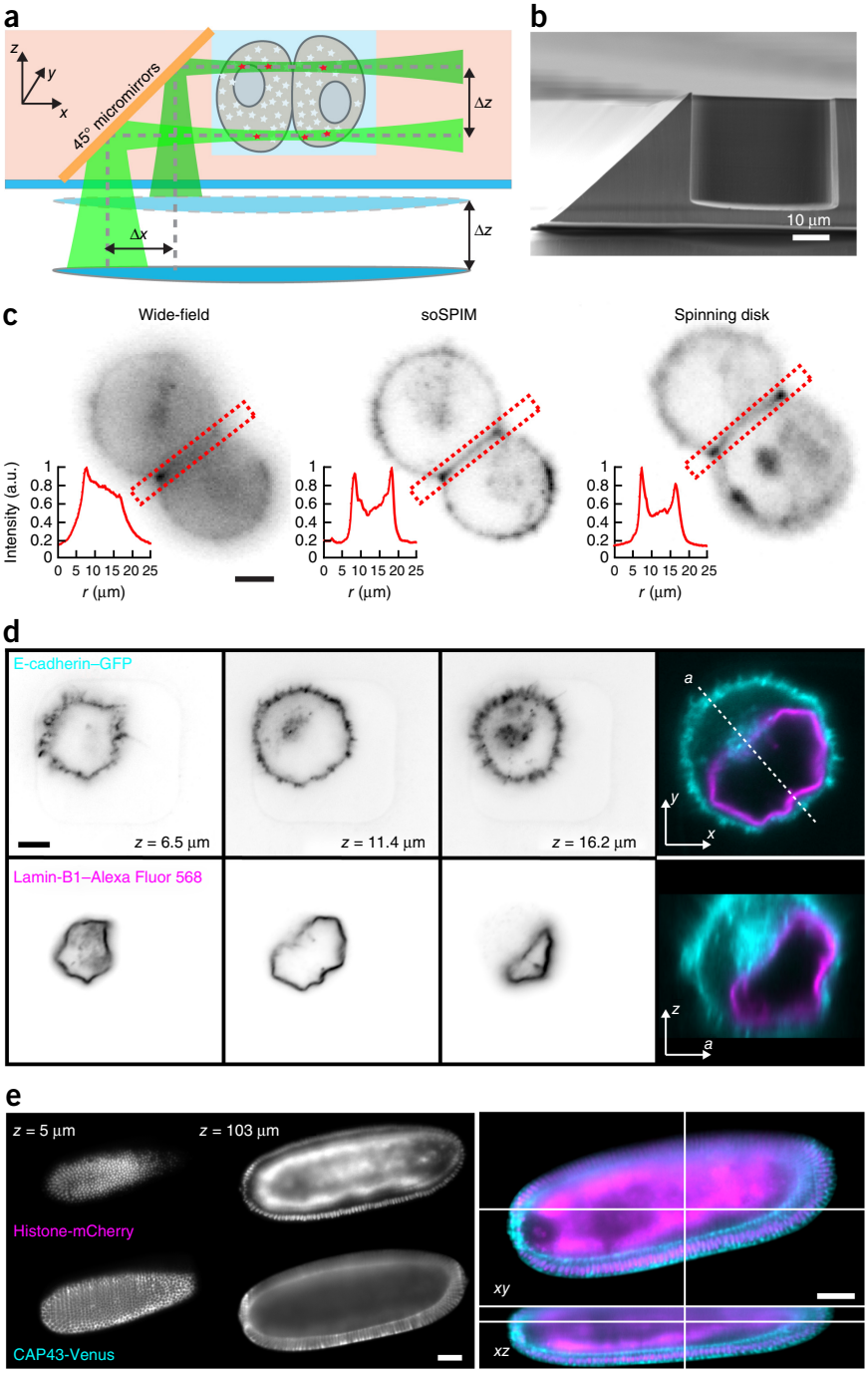

Figure 1 | Principle and 3D high-resolution capabilities of the soSPIM method. (**a**) Schematic representation of soSPIM. A light sheet is created by reflection from a 45° mirror. The excitation-beam displacement (Δx) along the mirror combined with the axial positioning of the objective (Δz) enables 3D-volume imaging. (**b**) Scanning electron microscopy image of a polymeric microcavity flanked by a mirror. (**c**) Comparison of the sectioning capabilities of wide-field, soSPIM and spinning-disk imaging of S180 cells expressing E-cadherin–GFP. Averaged line scans within the red dashed boxes are presented to illustrate the contrast gain. (**d**) Two-color soSPIM optical sections at the indicated depths of an S180 cell (expressing E-cadherin–GFP and immunolabeled with Lamin-B1–Alexa Fluor 568) within a 22 × 22 µm^2 microwell. The rightmost panel in the upper row shows the color combination of the soSPIM optical section at a depth of 11.4 µm (cyan, E-cadherin–GFP; magenta, Lamin-B1–Alexa Fluor 568). The rightmost panel in the lower row shows the orthogonal cross-section along *a*. (**e**) Two-color soSPIM optical sections of a *Drosophila* embryo expressing the nuclear protein histone-mCherry and the membrane protein CAP43-Venus imaged with a 20×/0.5-NA objective and a 4.3-µm-thick light sheet at 5 µm and 103 µm inside the embryo. Lateral and orthogonal views of the two-color images of the *Drosophila* embryo at the early stages of cellularization are shown (cyan, CAP43-Venus; magenta, histone-mCherry). Scale bars, 5 µm in **c** and **d** and 50 µm in **e**. n = 50 cells; n = 6 embryos.

Methods and **Supplementary Fig. 5**). We produced microcavities using sequential anisotropic and dry silicon etching techniques to culture cells and position them in the close vicinity of the mirrors. We replicated the silicon mold in a UV-curable polymer index matched with the cell-imaging medium. We sputtered gold and added additional polymeric protection to obtain mirrored surfaces with an optical quality of λ/50. Thousands of 40-µm-deep micromirrored wells fit on a 1.5H coverslip placed at the bottom of a 30-mm sterile petri dish. Cells grew in the resulting observation chamber. No further optical realignment was required to image multiple cells simultaneously.

We created observation chambers for embryos and large cell aggregates by casting Norland Optical Adhesive 73 onto commercial 45° microprisms (λ/20 optical quality). Gold sputtering onto the silicon-rubber imprint resulted in an opened mirror chamber mounted on an *ad hoc* holder that could be equipped with a sample rotation stage (**Supplementary Fig. 5b,c**).

To assess the sectioning capability of our technique, we imaged suspended live S180 cell doublets expressing E-cadherin–GFP through a 60×/1.2-NA water-immersion objective. The optical sectioning and contrast of soSPIM equaled that obtained with spinning-disc confocal microscopy (using a Yokogawa CSU-X1 scanner unit with 50-µm pinholes) (**Fig. 1c**) and revealed the characteristic zones of E-cadherin accumulation at the rim of the cell-cell junction[13]. We also achieved 3D multicolor acquisitions of cells expressing E-cadherin–GFP labeled with Lamin-B1–Alexa Fluor 568 at the single-cell level (**Fig. 1d**). The 5-µm raised bottom of the well, designed to prevent laser-beam clipping at the base of the mirror, allowed us to acquire thin adherent cell monolayers from basal to apical regions (**Supplementary Fig. 6a**). Microwell fabrication along the mirrors enabled simultaneous imaging of several cells in the camera's field of view and scanning of a whole dish without any realignment steps (**Supplementary Fig. 6b**). We were able to directly grow and image cell aggregates and monolayers *in situ* (**Supplementary Fig. 7a**). We used the thin and short light

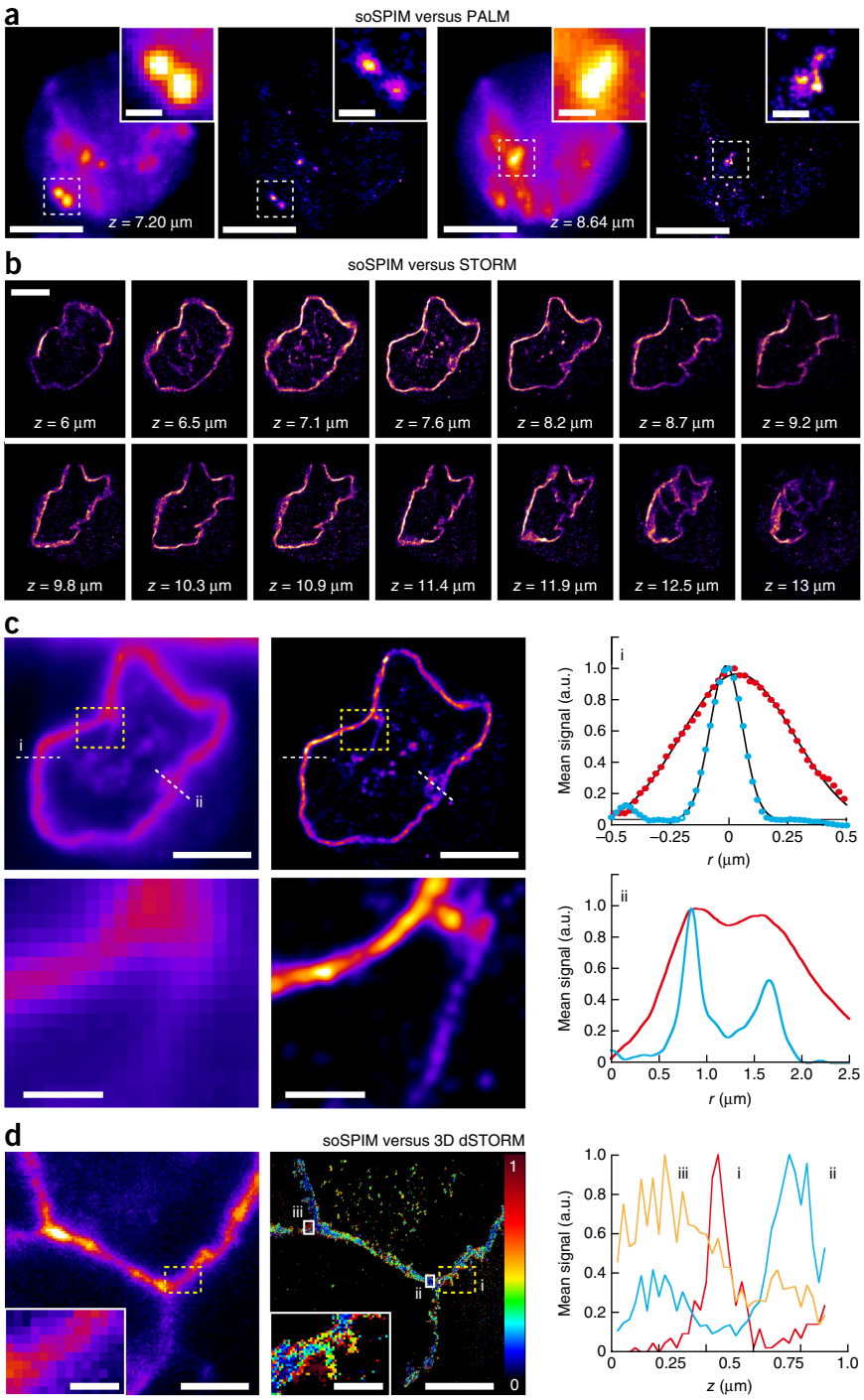

Figure 2 | 3D super-resolution capabilities of the soSPIM method. (**a**) High-resolution (two leftmost panels) and PALM super-resolution (two rightmost panels) images of a U2-OS cell nucleus expressing the nucleolus protein fibrillarin-Dendra2 at two different planes 1.44 µm apart (representative images; $n = 15$). The insets show zoomed views of the regions enclosed in the white dashed boxes. (**b**) Axial sections of 3D STORM super-resolution images acquired every 540 nm from 6 to 13 µm above the coverslip. Lamin-B1 in suspended S180 cells was labeled with the photoactivatable dye FLIP 565. (**c**) High- (left) and super-resolution (right) images of Lamin-B1 labeled with FLIP 565 7.6 µm deep in an S180 cell. Zoomed views of the boxed regions are presented (bottom row of panels), as well as the normalized intensity profiles along the nucleus membrane (white dashed lines; labels "i" and "ii" correspond to graph labels) for the high- (red circles or lines) and super-resolution (blue circles or lines) images. The black lines represent the Gaussian fits along the intensity profiles. We measured lamin-cortex thicknesses of 565 ± 9 nm (mean ± s.e.m.; full-width at half-maximum) for high-resolution images and 161 ± 10 nm for the super-resolution images. (**d**) 3D super-resolved axial sections acquired 12 µm above the coverslip of the cell-cell junction of an S180 cell doublet (labeled with E-cadherin–Alexa Fluor 647). Astigmatism-based single-molecule localization revealed the presence of filipodia that could not be seen on the high-resolution image. The image on the left shows the 3D color-coded super-resolution reconstruction. The 3D super-resolution image was reconstructed over a 1-µm-thick section. Insets show zoomed views of regions enclosed in dashed boxes. The mean intensity z profile of the boxed regions in the 3D super-resolution image exemplifies the axial resolution. dSTORM, direct STORM. Scale bars, 5 µm in **a**–**d** (1 µm in zoomed views).

sheet (1.6 × 26 µm) to image monolayers of large hepatocytes (>80 µm) using a multiview stitching approach that effectively lengthened the imaging field of view without compromising the sectioning capability (Online Methods and **Supplementary Fig. 7b–e**). Another application enabled by the soSPIM system was dual-color imaging of live embryos labeled with CAP43-Venus and histone-mCherry with a 20×/0.5-NA objective (using a light sheet 220 µm long × 4.3 µm thick) using lower magnification and larger mirrored chambers (**Fig. 1e**).

We then tested the capacity of our approach for 3D single-molecule-based nanoscopy, leveraging its high sectioning capability and high photon-collection efficiency. First, we imaged U2-OS cells expressing fibrillarin-Dendra2 using PALM[14,15] (**Fig. 2a**) with simultaneous photoconversion at 405 nm and excitation at 561 nm. We reconstructed the super-resolution images from 4,433 (left) and 2,137 (right) single-molecule localizations, extracted from 8,000 frames of 80 × 80 pixels acquired at 40 frames per second at 7.2 µm and 8.6 µm above the coverslip. This revealed subnuclear structures below the diffraction limit. The median number of photons collected above the background per localization event was 141.3, leading to a theoretical localization precision of about 40 nm (ref. 16) (**Supplementary Fig. 8**).

We were able to achieve 3D stochastic optical reconstruction microscopy (STORM)-like imaging[17–19] of the entire nuclear envelope of rounded S180 cells immunolabeled with FLIP 565 dye over 14 planes separated by 540 nm (**Fig. 2b** and **Supplementary Fig. 9a**). This illustrates the utility of soSPIM for dense, multiplane, 3D, super-resolution imaging that could not be achieved using wide-field illumination

(**Supplementary Fig. 9b**). We were able to clearly resolve the nuclear lamin-cortex folding arising from cell rounding. The cortex appeared to be 565 nm thick in high-resolution images, whereas it was 160 ± 10 nm thick (mean ± s.e.m.) in super-resolution reconstructions (**Fig. 2c**).

We implemented astigmatic-imaging-based 3D single-molecule localization (Online Methods) and imaged the cell-cell contact of S180 cells immunostained with Alexa Fluor 647–labeled antibody to E-cadherin using a standard direct-STORM buffer[18]. We were able to resolve filipodia with radial and axial sections of 200 nm next to the junction located 12 µm above the coverslip (**Fig. 2d**). We determined the empirical localization precision *in situ* by repeatedly imaging free dyes being spontaneously absorbed inside the polymeric matrix (**Supplementary Fig. 8c,d**). Using a 60×/1.2-NA water-immersion objective, we measured localization-precision values of 24 × 74 nm and 22 × 47 nm ($xy \times z$) for Alexa Fluor 647 and FLIP 565, respectively, at 5 µm above the coverslip. The localization precision decreased to between 80% and 50% of the 5-µm value at 40 µm above the coverslip (28 × 95 nm for Alexa Fluor 647) because of spherical aberrations. Such localization precision compares well to that of other super-resolution sectioning methods, including SPIM[7,10].

The soSPIM configuration enables broad modularity. Phase, differential interference contrast, wide-field, high-resolution and super-resolution imaging can be performed on the same microscope. Switching optical magnification does not involve any realignment. The requirement of perfect mechanical alignment of the two objectives used in traditional SPIM is obviated by the use of a single objective combined with software-controlled alignment of the light sheet along the mirror axis. Long-term stability is enhanced by the use of a single objective and the ability to implement the perfect-focus system built into inverted microscopes. In our study, the use of lower magnification and larger mirrored chambers enabled live imaging of *Drosophila* embryos during the first 3 h of embryo development (**Supplementary Video 1** and **Supplementary Fig. 10**). At this stage, soSPIM imaging of fly embryos did not equal that of the most specialized SPIM systems; however, the raw images were of reasonable quality for a single-side illumination. To improve image quality, we added a horizontal rotation stage that allowed multiview imaging (**Supplementary Fig. 11**, Online Methods and **Supplementary Video 2**). Finally, an unexplored advantage of our approach is its potential for studies of molecular trafficking and dynamics tens of micrometers away from the coverslip down to the single-molecule level. We believe that techniques for investigating collective protein dynamics on the basis of fluorescence (e.g., 2D fluorescence correlation spectroscopy and fluorescence recovery after photobleaching) or single-molecule trajectories (e.g., single-particle-tracking PALM[20] and uPAINT[21] (universal point accumulation for imaging in nanoscale topography)) could readily be implemented.

METHODS

Methods and any associated references are available in the online version of the paper.

Note: Any Supplementary Information and Source Data files are available in the online version of the paper.

ACKNOWLEDGMENTS

This work was supported by joint funding from the Ministère de l'Enseignement Supérieur et de la Recherche (ANR-10-INBS-04 FranceBioImaging), the Regional Council of Aquitaine and the Singapore National Research Foundation (NRF). V.V., G.G. and R.G. acknowledge financial support from the Mechanobiology Institute through an NRF grant. This research was conducted within the scope of the International Associated Lab LIA CAFS. The authors acknowledge A. Liew for help in the initial tests; P. Legros and C. Butler for help and feedback; S. Wolf and A. Wong of the Mechanobiology Institute for help editing the manuscript; C. Armouda and T. Saunders from the Mechanobiology Institute for help with *Drosophila* embryo imaging and for feedback; C. Viasnoff and G. Viasnoff for help with drawing conception; and K. Monier from ENS Lyon, W.J. Nelson from Stanford University and L. Hufnagel from EMBL for their kind gifts of stable fluorescent cell lines and a stable fluorescent embryo line. The authors thank Nikon France and Errol for loaning equipment.

AUTHOR CONTRIBUTIONS

R.G. performed the experiments and designed the optical setup. G.G. and R.G. designed and manufactured the micromirror chips. R.G. and A.A. imaged embryos. V.S. and V.V. came up with the original idea. J.-B.S., V.S. and V.V. conceived the experiments, supervised the work and contributed equally to the development of the project. R.G., G.G., V.V., V.S. and J.-B.S. contributed to the manuscript.

COMPETING FINANCIAL INTERESTS

The authors declare competing financial interests: details are available in the online version of the paper.

1. Tokunaga, M., Imamoto, N. & Sakata-Sogawa, K. *Nat. Methods* **5**, 159–161 (2008).
2. Huang, B. *et al. Science* **319**, 810–813 (2008).
3. Pavani, S.R. *et al. Proc. Natl. Acad. Sci. USA* **106**, 2995–2999 (2009).
4. Juette, M.F. *et al. Nat. Methods* **5**, 527–529 (2008).
5. Shtengel, G. *et al. Proc. Natl. Acad. Sci. USA* **106**, 3125–3130 (2009).
6. Cisse, I.I. *et al. Science* **341**, 664–667 (2013).
7. Cella Zanacchi, F. *et al. Nat. Methods* **8**, 1047–1049 (2011).
8. Planchon, T.A. *et al. Nat. Methods* **8**, 417–423 (2011).
9. Wu, Y. *et al. Proc. Natl. Acad. Sci. USA* **108**, 17708–17713 (2011).
10. Gebhardt, J.C. *et al. Nat. Methods* **10**, 421–426 (2013).
11. Chen, B.C. *et al. Science* **346**, 1257998 (2014).
12. Hu, Y. *et al. Opt. Nanoscopy* **2**, 7 (2013).
13. Engl, W. *et al. Nat. Cell Biol.* **16**, 587–594 (2014).
14. Betzig, E. *et al. Science* **313**, 1642–1645 (2006).
15. Hess, S.T., Girirajan, T.P. & Mason, M.D. *Biophys. J.* **91**, 4258–4272 (2006).
16. Thompson, R.E., Larson, D.R. & Webb, W.W. *Biophys. J.* **82**, 2775–2783 (2002).
17. Rust, M.J., Bates, M. & Zhuang, X. *Nat. Methods* **3**, 793–795 (2006).
18. Heilemann, M. *et al. Angew. Chem. Int. Edn. Engl.* **47**, 6172–6176 (2008).
19. Fölling, J. *et al. Nat. Methods* **5**, 943–945 (2008).
20. Manley, S. *et al. Nat. Methods* **5**, 155–157 (2008).
21. Giannone, G. *et al. Biophys. J.* **99**, 1303–1310 (2010).

ONLINE METHODS

soSPIM microscope. In this study, the soSPIM components (**Supplementary Fig. 1**) were mounted on a conventional inverted microscope (Nikon Ti-E). The sample holder was placed on an axial-translation piezo stage (P-736 PInano, Physik Instrumente; 200-µm travel range). The fluorescence signal was collected by the microscope tube lens through the same objective used for excitation and captured with either an EM-CCD (electron-multiplying charge-coupled device) camera (Evolve 512, Photometrics) or an sCMOS (scientific complementary metal-oxide semiconductor) camera (Neo 5.5, Andor). When combined with a high-NA objective, an EM-CCD camera provides sufficient sensitivity for single-molecule-based super-resolution imaging. The large field of view of the sCMOS camera can be used both to position and image the 45° micromirror according to the sample and to image larger samples (when used with lower-magnification objectives). The microscope was enclosed in an environmental chamber (Okolab) that enabled the operator to control the temperature (between 28 °C and 37 °C) and the CO_2 concentration for live-cell imaging. The acquisition was steered by MetaMorph software (Molecular Devices).

soSPIM laser beam–steering system. Illumination lasers (405 nm (200 mW; Errol), 488 nm (200 mW; Coherent), 561 nm (200 mW; Coherent) and 635 nm (150 mW; Errol)) were collimated and colinearly combined via dichroic beam splitters and coupled into a single-mode optical fiber for spatial filtering and convenient alignment. An acoustic-optic tunable filter (AOTF) was used to select one or several wavelengths, control intensities and provide on-off modulation. The maximum laser power at the optical fiber output was less than 50 mW for super-resolution imaging and less than 10 mW for high-resolution 3D imaging. Light-sheet illumination enables optimization of the energy-density repartition in the imaged plane, leading to lower laser-intensity requirements than for other 3D-imaging modes. The laser beam was expanded to a 2-mm Gaussian beam using an achromatic reflective collimator (RC02APC-P01, Thorlabs). A laser-beam telescopic expander (here AC254-050-A, Thorlabs (focal length of 50 mm), and AC254-75-A, Thorlabs (focal length of 75 mm)) providing 1.5× magnification of the excitation beam may be inserted into the optical path to vary the diameter, or NA, of the excitation beam.

The laser beam was sent to an *x*-axis galvanometric mirror (XG) (Pangolin SCANMAX 506 actuators with dielectric Chroma mirrors), which was imaged onto a conjugated *y*-axis galvanometric mirror (YG) by relay lenses (AC254-050-A, Thorlabs; focal length of 50 mm for both lenses). The laser beam was then imaged on a focus-tunable lens (TL) (Custom EL-30-10, Optotune; focal lens from −80 mm to +1,000 mm) by relay lenses (AC245-050-A, Thorlabs; focal length of 50 mm for both lenses). The focal length of the TL was constantly maintained by the built-in feedback-loop system. The TL was finally imaged and centered on the back focal plane (BFP) of the microscope's objective, which can be a high-NA microscope objective (here a CFI Plan Apochromat VC 60×/1.2-NA water-immersion objective or a CFI Plan Apochromat VC 100×/1.4-NA oil-immersion objective, Nikon) or a low-magnification objective (here a CFI Plan Fluor 10×/0.3-NA, CFI Plan Fluor 20×/0.5-NA or CFI Plan Fluor 40×/0.75-NA objective, Nikon), by a third telescope (AC254-150-A, Thorlabs, and the tube lens of the microscope; focal length of 150 mm for both lenses).

The XG and YG galvanometers and the TL were precisely aligned and conjugated to the BFP of the objective. This was essential to ensure that the light sheet was perpendicular to the optical axis of the microscope objective after reflection onto the 45° mirror regardless of its reflection position. The conjugation was achieved by collimating the laser beam after each relay lens with a shearing interferometer (shear plate SI035, Thorlabs) mounted in place of the microscope objective. We aligned the optical elements with the center of the objective BFP by means of iterative centering steps between the BFP and the image of the beam reflected off a flat mirror that was positioned perpendicular to the microscope's optical axis at the BFP. Small deviations from the 45° angle of the micromirror with respect to the optical axis of the microscope objective were compensated for by slightly decentering the laser beam on the BFP without modifying the conjugations.

For single-molecule-based super-resolution microscopy, a cylindrical lens (ACY254-150-A, Thorlabs; focal length of 150 mm) was inserted into the excitation path. This enabled the laser beam to focus in a single direction on the BFP of the objective, creating a continuous illumination light sheet without scanning of the laser beam on the mirror. The cylindrical lens could be mounted in a rotational mount to align the largest dimension of the light sheet with the long axis of the mirror when needed.

The galvanometric mirrors were controlled using Lasershow Designer (Pangolin Laser Systems). Calibration and image acquisition were performed using MetaMorph software (Molecular Devices).

For initial calibration of the steering direction along the mirror, we used the sCMOS camera. A scanning frame parallel to the mirror axis was defined as the *y*-axis. *z*-scanning was achieved by translating the scanning direction orthogonal to the mirror axis (*x*-direction). For whole-embryo imaging, the sCMOS camera was also used for the acquisition. For super-resolution microscopy, the EM-CCD camera was used, in which case the mirror lay outside the field of view (FOV) of the EM-CCD but was still located within the objective's FOV.

Beam characterization and calibration. We calculated the profile of the excitation beam, which depends on its NA or diameter in the BFP, by directly imaging the excitation beam through a fluorescent solution (fluorescein, 1 µg/mL in water) after reflection by the 45° mirror (**Supplementary Fig. 2b**). The beam cross-section profiles were measured by intensity line scanning along the direction perpendicular to the light propagation. Gaussian fittings of these profiles enabled retrieval of the thickness of the beam at various positions (**Supplementary Fig. 2b**). We obtained the profile of the excitation beam by plotting its thickness with respect to its position along the light propagation and fitted it with a Gaussian beam-propagation equation (**Supplementary Fig. 2c**):

$$\omega(x) = \omega_0\sqrt{1+\left(\frac{x-x_0}{Z_R}\right)^2} \quad (1)$$

Subsequently, the waist ω_0 of the beam, representing the minimum thickness of the light sheet; the Rayleigh length Z_R, corresponding to half the size of the FOV of the light sheet; and the position of the beam focalization x_0 along the propagation

direction were extracted and compared to the theoretical relation between ω_0 and Z_R (**Supplementary Fig. 2d**).

$$\omega_0 = \sqrt{\frac{\pi Z_R}{\lambda}} \quad (2)$$

The light-sheet thickness and FOV depend on the size of the excitation beam at the objective's BFP and the NA of the objective. For high-NA objectives, used for high- and super-resolution imaging, we measured, at a wavelength of 561 nm, a thickness (at full-width at half-maximum) of 1.6 ± 0.2 µm (mean ± s.e.m.) for an FOV of 25.7 ± 1.0 µm with a 3-mm beam diameter at the BFP of a 60×/1.2-NA objective and a thickness of 1.2 ± 0.09 µm for an FOV of 10.8 ± 0.8 µm for a 100×/1.3-NA objective. For low-magnification objectives, used for imaging thick samples, we measured thicknesses of 5.2 ± 0.8 µm, 4.3 ± 0.6 µm and 3.7 ± 0.5 µm for FOVs of 264 ± 12 µm, 220 ± 10 µm and 160 ± 10 µm for 10×, 20× and 40× objectives, respectively (**Supplementary Fig. 2d**).

Extraction of the beam parameters x_0, ω_0 and Z_R enabled calibration of the different components of the system. A first calibration was performed to ensure the superposition of the objective focal plane with the light-sheet plane for 3D imaging. For each displacement dx of the light sheet along the mirror x-axis, the light-sheet z-position was measured, evaluating the axial position minimizing ω_0. Repeating this process for several dx displacements enabled extraction of the corresponding displacements dz to be applied to the z-stage when we moved the light sheet along the mirror's x-axis (**Supplementary Fig. 12a**). For the 60× water-immersion objective and the 40×, 20× and 10× air objectives, we measured coefficients dz/dx of 0.76, 0.65, 0.64 and 0.69, respectively. These coefficients differed from 1.0 because of the index mismatch between the immersion medium of the objectives and the imaging medium. Indeed, such a mismatch, which can induce an axial shift between the actual and the nominal focal-plane positions[22], needs to be taken into account for optimal 3D-volume imaging.

To calibrate the defocus system, we extracted the focalization position of the beam x_0 along the propagation direction (**Supplementary Fig. 12b**). There is a linear dependence between the current sent to the lens and the light-sheet position along the x-axis, and we used this relation to precisely position the light sheet on the sample according to its distance from the mirror.

Finally, determining the x_0 drift for various defocus strengths applied to the divergent lens with respect to the objective's axial displacement allowed us to compensate for this drift in order to perform optimal 3D-volume imaging (**Supplementary Figs. 3** and **12c**). This compensation ensured that the light-sheet displacement was less than 2% for imaging planes ranging from 0 to 40 µm for high-NA objectives and less than 5% for imaging planes ranging from 0 to 300 µm for low-magnification objectives.

Microfabrication process for sterile chips. The fabrication process for the silicon chips displaying 45° micromirror surfaces and microwells is represented in **Supplementary Figure 5a**. Micromirroring surfaces were produced in (100)-oriented silicon wafers by anisotropic etching in an alkaline solution (tetra-methyl ammonium hydroxide (TMAH)). By tuning the etching conditions (i.e., alkaline solution, surfactant concentration and etching-bath temperature), we were able to obtain a slower etching rate for the (110) crystalline plane than for the (100) crystalline plane. Etching in a preferential direction occurs because of the action of a surfactant that acts as a preferential protection layer[23–25]. If the areas cleared for the etching on the wafer are oriented at a 45° angle from the <110> reference direction of the wafer, the exposed (110) planes are preserved, and the progressive etching of (100) planes reveals a cavity flanked by exactly 45° slanted surfaces. Using a solution of 25% TMAH in water plus 100 ppm Triton X (Sigma Aldrich) as a surfactant at 80 °C for 2 h, we achieved etching of approximately 45-µm-deep grooves with 45° walls. Microwells of different sizes (22 × 22 µm^2, 24 × 24 µm^2, 40 × 40 µm^2 and 60 × 300 µm^2) aligned with the 45° slanted surfaces were then created via a deep reactive-ion etching process through openings in SU-8 negative tone resist.

The silicon wafer was replicated into a secondary mold made of polydimethylsiloxane (PDMS) (Sylgard 184, Dow Corning), mixed 10:1 with its curing agent and then cured at 80 °C for 2 h after 30 min of outgassing (**Supplementary Fig. 5a**). A capillary process was used to reproduce from the PDMS secondary mold on a clean 1.5H coverslip with the UV-curable and index-matched polymer, which was cured by immersion in water for 12 min under UV (500-W arc lamp, 66902, Newport). After the PDMS mold was peeled off, the plastic chips were coated with a thin layer of gold by plasma sputtering in a vacuum chamber (JFC-1600 Auto Fine Coater, JEOL) to make the 45° surfaces reflective. Typically, 70%–90% reflectivity is achieved with this method. After metallization, the mirrors were protected with a layer of UV-curable polymer (NOA 73, Norland Products), which was applied by capillary flow while the microwells were protected by a flat piece of PDMS; the optical adhesive was then cured by a 1-min exposure to UV light. Finally, the flat PDMS piece was peeled off, and the unprotected metal coating was removed by wet etching (gold etchant, 651818, Sigma). The coverslips were finally attached to a bottom-free 35-mm plastic dish (**Supplementary Fig. 4a**) that allowed for easy surface passivation (overnight incubation with 0.2× Pluronic solution (F127, Sigma)) and/or functionalization (1 h of incubation with fibronectin (Sigma)), as well as cell culture within the chip.

Fabrication process for fly embryo chips. The fabrication of millimeter-sized mirrors for imaging thick samples, such as *Drosophila* embryos, was done using soft microfabrication processes as described in **Supplementary Figure 5b**. A 45° microprism with λ/20 surface quality (8531-602, Precision Optics Corporation) 0.7–3 mm in size positioned on a flat surface flanked by PDMS sheets was replicated in a UV-curable polymer (NOA-73, Norland Products). The inner surface of the prism imprint was then coated with a gold layer by plasma sputtering in a vacuum chamber (JFC-1600 Auto Fine Coater, JEOL). The metallized prism imprint was finally assembled on a coverslip for imaging. The extremities of the prism imprint were opened to ensure oxygen and nutriment exchange with the medium. These openings also enabled the insertion of a capillary made in an index-matched polymer (OF-134, MyPolymer) between the 45° mirrors (**Supplementary Fig. 5** and **Supplementary Video 1**). This polymeric capillary was fabricated as follows: a blunt needle (27-gauge) with a 600-µm outer diameter was inserted into a glass capillary tube (900-µm inner diameter). The system

doi:10.1038/nmeth.3402

tube was subsequently filled with OF-134 and UV cured. Once cured, the polymeric part was partially pulled out of the glass capillary. The needle was subsequently used as a piston to suck in the fly embryos, as is usually done in traditional SPIM systems. An embryo was positioned at the very end of the polymeric tube. The index matching of the tube with the surrounding medium precluded any light distortion because of the tube's cylindrical shape. The concentric tubes were subsequently introduced in a fixed sheath that was aligned with the mirror axis and served as a rotation guide. The tube was connected to a computer-controlled step-rotation motor (Stepper Bee control module) with a precision of 0.17°. The rotation speed was 90° per 5 s. The precise rotation of the capillary by a multistep rotation motor eventually enabled the acquisition of multiple views of a sample mounted within the index-matched capillary. Alternatively, a perfluorinated elastomer tube could probably be used.

Cell culture and transfection. S180 cells stably expressing E-cadherin–GFP were a kind gift from J.-P. Thiery (Institute of Molecular Cell Biology, A*STAR, Singapore). MDCK cells stably expressing actin-GFP were a kind gift from W.J. Nelson (Stanford University, CA).

A clonal U2-OS stable cell line expressing pDendra2-fibrillarin (Evrogen, FP826-d; Dendra2 fused to the N terminus of fibrillarin) was established using a U2-OS osteosarcoma cell line (ATCC HTB-96). Cells were maintained at 37 °C in a 5% CO_2 humidified incubator. One day before transfection, six-well dishes were plated with 1.2×10^5 cells per dish. Cells were transfected in complete Mc (CM-Mc) medium (McCoy's 5a medium (Life Technologies) supplemented with 10% inactivated fetal bovine serum (FBS) (Sigma), 1% non-essential amino acids (Life Technologies), 1% GlutaMAX (Sigma) and 1% penicillin-streptomycin (Sigma)) using jetPRIME DNA transfection reagent (Polyplus Transfection) in a 1:2 ratio. The following day, transfected cells were transferred into 15-cm-diameter culture dishes. Clone selection was then carried out using CM-Mc medium containing 0.4 mg/mL of G418. Ten to fifteen days after transfection, clones were chosen under a fluorescence microscope to ensure reliable and proper fluorescence localization. Selected clones were then isolated and transferred to 24-well dishes for expansion and frozen in culture medium containing 10% dimethylsulfoxide. Further selection with G418 was not done after the next thawing; no loss of fluorescence was noted.

Hepatocytes were isolated from male Wistar rats by a two-step *in situ* collagenase perfusion method. Animals were handled according to the Institutional Animal Care and Use Committee (IACUC) protocol approved by the IACUC of the National University of Singapore. With a yield of $>10^8$ cells per rat, hepatocyte viability was determined to be >90% by Trypan Blue exclusion assay.

S180 and MDCK cells were cultured in high-glucose Dulbecco's modified Eagle's medium (Sigma) supplemented with 10% FBS (Sigma), 1% GlutaMAX (Sigma) and 1% penicillin-streptomycin (Sigma). U2-OS cells were cultured in CM-Mc medium. Freshly isolated rat hepatocytes were cultured in William's E culture medium (Sigma) supplemented with 1% L-glutamine (Sigma), 1 mg/ml BSA, 0.3 µg/ml insulin (Sigma), 100 nM dexamethasone (Sigma), 50 µg/ml linoleic acid (Sigma), 100 units/ml penicillin (Sigma) and 100 mg/ml streptomycin (Sigma).

Transfection of S180 cells was done using lipofectamine reagent (Life Technologies). A first mix of 150 µL of OptiMEM medium (Sigma) with 5 µL of lipofectamine and a second mix of 150 µL of OptiMEM and 1 µg of DNA plasmid (FTractin-RFP) were made and allowed to incubate for 5 min. The two mixes were then combined and allowed to incubate for 15 min. In the meantime, cells were washed twice in PBS and immersed in 700 µL of OptiMEM medium. The DNA mix was then poured on the cells and allowed to incubate for 4 h at 37 °C and 5% CO_2. After incubation, the OptiMEM medium was removed and replaced with common growth medium. The cells were used the day after transfection as described below.

Cell seeding. The day before being seeded into the microwells, S180 cells were cultured in 35-mm plastic dishes to ensure 70% confluence on the day of seeding. The cells were then washed twice with 1× PBS (Sigma) and immersed in 1 mL CO_2-independent cell-growth medium (Sigma), which was also used as the imaging medium. We detached S180 cells mechanically by pipetting the growth medium several times and then placed them in an incubator for 10 min. Other cell lines (U2-OS, MDCK and primary hepatocyte) were detached by treatment with 0.2× Trypsin (Sigma) on the day of seeding, placed in growth medium and allowed to recover for 10 min in the incubator.

For microwell seeding, 500,000 cells were deposited onto the microwells and placed in the incubator for 10 to 15 min to allow the cells to fill the microwells. The unattached cells were removed by rinsing with PBS, and growth medium was added. This seeding step could be repeated two to three times, depending on the filling of the microwells by the cells. Finally, the dish containing the microwells was incubated at 37 °C and 5% CO_2. For long-term culture, the growth medium was changed on a daily basis.

Cell fixation and immunostaining. All the fixation and staining steps were done directly in the dish containing the microwells, to facilitate handling of the cells. U2-OS cells were fixed in −20 °C methanol for 5 min after the growth medium had been washed away with PBS. The cells were then washed three times in PBS and stored in PBS until imaging.

For Lamin-B1 staining, S180 cells were washed two times with PBS and fixed in 4% paraformaldehyde solution (Sigma) for 10 min. After being washed with PBS, the cells were permeabilized in 0.1% Triton X-100 solution for 5 min and then blocked with 3% BSA in PBS (Sigma) for 30 min to avoid unspecific labeling. The cells were then labeled sequentially with primary rabbit anti–Lamin-B1 (1:500, ab16048, Abcam) and FLIP 565 (1:200, 2-0012-202-1, Abberior) for 1 h each. The cells were finally washed with PBS and stored in PBS at 4 °C.

For E-cadherin staining, S180 cells were allowed to incubate at 37 °C for 1.5 h in the microwells to enable the formation and maturation of cell-cell junctions. The growth medium was then removed, and 100 µL of the primary antibody labeled with Alexa Fluor 647 (1:200, anti-CD324 Alexa Fluor 647, 51-3249, eBioscience) was deposited into the microwells and allowed to incubate for 30 min at 37 °C. After being rinsed with growth medium, the microwells were washed two times with PBS and fixed in 4% paraformaldehyde solution for 10 min. The wells were finally washed with PBS and stored in PBS at 4 °C.

For actin staining, hepatocytes cultured for 48 h in microwells were fixed in 4% paraformaldehyde at 37 °C for 30 min. After fixation, the cells were rinsed by PBS and permeabilized for 30 min in PBST (0.1% Triton X in PBS). The permeabilized cells were blocked with 1% BSA in PBST for 4 h at 4 °C and incubated with Alexa Fluor 488 phalloidin (1:200, A12379, Life Technologies) for 1 h at room temperature. After being rinsed with PBST, cells were stored in PBS at 4 °C.

Imaging of single cells, cell doublets and cell aggregates. For live-cell imaging, the microwells were rinsed two times and immersed in an imaging medium (CO_2-independent medium without phenol red, supplemented with 10% FBS; Sigma). Fixed cells were immersed in PBS for image acquisition.

The micro-fabricated chip was placed on the microscope stage, and a 60×/1.2-NA water-immersion objective was used for imaging (CFI Plan Apochromat VC). First, the scanning directions of the galvanometer mirror for both the creation and the axial displacement of the light sheet were determined according to the mirror orientation in the FOV of the objective. The appropriate defocus strength was then determined according to the distance of the sample from the micromirror. 3D-volume imaging was finally performed using MetaMorph software (Molecular Devices), synchronizing the acquisition with the movements of the galvanometric mirrors, the defocus system and the axial position of the objective.

For imaging of single cells and cell doublets within $22 \times 22\,\mu m^2$ and $24 \times 24\,\mu m^2$ microwells, a light sheet with a thickness of $1.5 \pm 0.2\,\mu m$ and an FOV of $28.5 \pm 1.0\,\mu m$ was used. For cell-aggregate imaging within $40 \times 40\,\mu m^2$ microwells, a light sheet with a thickness of $1.9 \pm 0.2\,\mu m$ and an FOV of $36.8 \pm 1.0\,\mu m$ was used.

For cell-aggregate imaging in $60 \times 300\,\mu m^2$ microwells, an *x*-axis scanning system of a light sheet with a thickness of $1.5 \pm 0.2\,\mu m$ and an FOV of $28.5 \pm 1.0\,\mu m$ had to be implemented to increase the imaging field while optimizing the axial resolution and reducing the shadowing effects. Three images at each plane were taken, and we defocused the light sheet by 20 µm each time to cover the whole width of the well with a 28-µm-long light sheet. The three images were then merged using three masks centered on the position of the light sheet (**Supplementary Fig. 7b–e**). The masks were defined with the relation

$$Max\left\{0,\left[\tanh\left(\frac{1-q}{s}\right)\right]\times\left[1-\tanh\left(\frac{1-q+w}{s}\right)\right]\right\} \quad (3)$$

where q represents the position of the light sheet, w is the length of the light sheet and s is the slope of the filter border.

Single-molecule-based super-resolution imaging. Samples labeled with organic dyes or photoconvertible proteins were imaged on an inverted microscope (Nikon TiE) adapted for soSPIM equipped with a 60×/1.3-NA objective, a 1.5× magnification lens and a perfect-focus system (PSF3, Nikon) allowing long-term acquisition tens of micrometers above the coverslip.

For samples labeled with Alexa Fluor 647, imaging was performed in an extracellular solution containing reducing and oxygen-scavenging compounds, according to the direct STORM protocol[17], in a closed chamber. At the beginning of the experiment, the ensemble fluorescence of Alexa Fluor 647 was first converted into a dark state using a 640-nm laser. Once the ensemble fluorescence was converted into the desired density of single molecules, the laser power was reduced. 10,000 to 20,000 images per *z*-plane were recorded continuously in streaming mode at 66 frames per second with the EM-CCD camera (Evolve 512, Photometrics) through a quad-band filter (ZET 405/488/561/640, Chroma). For Dendra2- and FLIP 565–labeled samples, imaging was performed in PBS at room temperature. A 405-nm photoactivation laser and a 561-nm excitation laser were used and directed toward the objective with a custom dual-band cube filter (excitation: ZET 405/488/561x triple-band laser; dichroic: ZT 405/488/561 rpc triple-band laser; emission: ZET 488/561 double-band laser; all from Chroma). The laser powers were tuned through the AOTF to optimize the fluorescent signal and the single-molecule density per image. The acquisition sequence was steered using MetaMorph software. 2D and 3D single-molecule localization and super-resolution image reconstruction were achieved using the WaveTracer module (Molecular Devices) with a combination of wavelet-based localization and anisotropic Gaussian fitting methods[26,27]. 3D localization was performed using an N-STORM astigmatic lens (Nikon) located in front of the EM-CCD camera. For super-resolution imaging over a thickness of several micrometers, super-resolution acquisition sequences were taken every 500 nm along the *z*-axis.

Calibration of the astigmatism-based point spread function deformation for 3D localization was performed directly within the microfabricated chip. Free dyes were absorbed within the polymer during the immune-staining steps, so that no additional fabrication steps were required to insert these dyes for calibration purposes. Imaging through the polymer in the soSPIM configuration enabled imaging of stable dyes protected from oxygen bleaching for easy performance evaluation and 3D astigmatism calibration at any depth inside the sample (**Supplementary Fig. 8c**).

For astigmatism calibration, *z*-stacks of single emitters located at 10 to 15 µm above the coverslip were acquired with 50-nm *z*-steps over 2 µm and analyzed using anisotropic Gaussian fitting[2,28] with the WaveTracer module.

For experimental-localization performance evaluation, 4,000 images of sparsely distributed single molecules embedded within the chip polymer were acquired in streaming mode with a signal-to-noise ratio similar to that for the single-molecule signal within cells. Repeated localization of these stable, oxygen-free single molecules enabled the localization of single molecules several times ($n > 72$) for the evaluation of localization precision. This allowed easy evaluation of the 3D resolution performance of the soSPIM microscope at the exact depth of the imaged samples. The detection of 35 single molecules localized at least 128 times at 5 µm and 40 µm above the coverslip gave localization-precision values of 23.9 nm and 27.8 nm, respectively, in *xy* and of 73.6 nm and 94.9 nm, respectively, in *z* over a total thickness of 780 nm around the objective focal plane for Alexa Fluor 647 dyes (**Supplementary Fig. 8c,d**). For FLIP 565, the detection of 23 single molecules localized at least 72 times gave localization-precision values of 21.5 nm in *xy* and 46.3 nm in *z* (**Supplementary Fig. 8d**).

Culture and imaging of *Drosophila* embryos. Genetically modified adult *Drosophila* flies expressing the membrane protein CAP43-Venus and the nuclear protein histone-mCherry[29] were enclosed in an embryo collection bottle composed of a standard

doi:10.1038/nmeth.3402

grape-juice agar egg-collection plate. The collected eggs were immersed in Halocarbon oil 27 (Sigma) for identification of the embryonic development stage. We selected between 10 and 15 embryos at the early cellularization stage and transferred them to a small piece of humidified absorbent paper. *Drosophila* embryos were immersed in 100% bleach solution for 60 s for chorion removal and then washed three times with water.

For imaging, the metallized right-angle prism imprint in polymer was half-filled with a 1% wt/vol low-melting-point agar gel (Sigma). The *Drosophila* embryos were deposited onto the gel under a binocular microscope, and the polymer imprint was filled with agar gel. Finally, the right-angle prism imprint was pressed on a coverslip and sealed with silicon grease for imaging with the soSPIM system. To prevent the formation of an air layer between the coverslip and the agar gel that could lead to a refractive-index mismatch, we deposited a drop of water onto the gel before the coverslip was sealed on it. The coverslip was mounted in a chamber filled with PBS on the inverted microscope adapted for soSPIM imaging. Imaging was performed using a 10×/0.3-NA objective or a 20×/0.5-NA objective. 488-nm and 561-nm lasers were directed toward the samples with a custom dual-band cube filter (excitation: ZET 405/488/561x triple-band laser; dichroic: ZT 405/488/561 rpc triple-band laser; emission: ZET 488/561 double-band total internal reflection fluorescence laser; all from Chroma), and acquisitions were done with the large-FOV sCMOS camera. Time-lapse acquisitions were performed at room temperature with a 20×/0.5-NA objective and a light sheet 4.3 ± 0.6 µm thick and 220 ± 10 µm long. 35-µm *z*-stacks with a 1.35-µm *z*-step were acquired (150 s each for 220 min). It has to be noted that the embryo line used had been selected for its brightness but not for its health; we observed several events of cellular apoptosis during embryo development (**Supplementary Fig. 10a**). Nevertheless, the embryos reached the gastrulation stage each time they were imaged, demonstrating their viability under soSPIM imaging.

22. Visser, T.D., Oud, J.L. & Brakenhoff, G.J. *Optik (Stuttg.)* **90**, 17–19 (1992).
23. Strandman, C., Rosengren, L., Elderstig, H.G.A. & Backlund, Y. *J. Microelectromech. Syst.* **4**, 213–219 (1995).
24. Barycka, I. & Zubel, I. *Sens. Actuators A Phys.* **48**, 229–238 (1995).
25. Resnik, D., Vrtacnik, D., Aljancic, U., Mozek, M. & Amon, S. *J. Micromech. Microeng.* **15**, 1174–1183 (2005).
26. Kechkar, A. *et al. PLoS One* **8**, e62918 (2013).
27. Izeddin, I. *et al. Opt. Express* **20**, 2081–2095 (2012).
28. Holtzer, L., Meckel, T. & Schmidt, T. *Appl. Phys. Lett.* **90**, 053902 (2007).
29. Martin, A.C. *et al. J. Cell Biol.* **188**, 735–749 (2010).